euspen's 26th International Conference & Exhibition, Krakow, PL, June 2026

www.euspen.eu

Robust design of diffractive optical elements for anticounterfeiting mould texturing

Marco Sorgato[1,*]; Giacomo Baruffa[1]; Giovanni Lucchetta[1]; Enrico Savio[1]

[1]*Department of Industrial Engineering, University of Padova, via Gradenigo 6/A, 35131 Padova, Italy*

[*]*Marco.sorgato@unipd.it*

Abstract

Counterfeiting significantly affects injection molding, a technology widely used for high-volume, low-cost production. Developing robust, cost-effective anti-counterfeiting features that can be directly integrated into injection-molded polymer components is a relevant industrial challenge. Diffractive optical elements (DOEs) are promising candidates, as they enable the projection of holographic images combining easy visual authentication with complex optical signatures. This work presents a systematic prototyping framework for phase-only DOEs using two-photon polymerization lithography. The framework aims to identify geometries compatible with the spatial resolution and accuracy of industrial mold texturing processes. In the first phase, the influence of pixel pitch and phase discretization levels on holographic image quality was evaluated using contrast transfer function and mean-squared-error metrics. An optimal configuration with a 7 µm pixel pitch and 3 phase levels was identified, balancing image quality and manufacturability. In the second phase, the robustness of this configuration was assessed by introducing controlled defects in pixel height and pitch. Results show that although such defects affect hologram quality, functional performance remains within error ranges compatible with state-of-the-art mold texturing technologies. Overall, the study provides quantitative guidelines for integrating DOE-based holographic anti-counterfeiting features into injection-molded components.

Diffractive optical elements; surface functionalization; two-photon polymerization; prototyping.

1. Introduction

Counterfeiting is a growing global concern, and injection molding (IM) is particularly vulnerable due to its high-volume, low-cost production model [1]. This motivates the development of cost-effective anti-counterfeiting solutions that can be directly integrated into IM components. A promising approach is to replicate diffractive micro- and nanostructures from textured molds to generate structural-color tags [1]. However, effective protection should combine easily recognizable features with elements that are difficult to interpret and replicate, such as diffractive optical elements (DOEs) implemented as computer generated holograms. DOEs exploit micro- or nanoscale features to manipulate light and project holographic images under controlled illumination, with phase-only transmission-mode DOEs generally preferred for their high efficiency [2,3].

Although DOEs are compatible with IM due to the absence of undercuts, their direct integration into molds is limited by the resolution of current texturing technologies [4]. DOEs are usually produced via lithographic processes [2,3], which, despite providing high spatial resolution, are unsuitable for direct mold texturing due to the costs related to mask fabrication and the need to operate in a vacuum. Moreover, such processes cannot be directly applied to standard mold materials [5].

Finally, DOE performance is highly sensitive to dimensional inaccuracies. Errors in pixel height and pitch directly affect phase modulation and diffraction angles [6,7]. Consequently, the precision and accuracy limitations of the texturing processes significantly impact the quality of the projected images [5]. While previous studies have numerically analyzed the influence of fabrication defects on diffraction efficiency, experimental studies linking inaccuracies to holographic image quality remain limited, particularly in the context of the IM process chain [5–7].

Overall, integrating DOEs into injection molds requires a quantitative understanding of the spatial resolution required to preserve holographic image quality and of the effects of process-induced inaccuracies on DOE functionality, to define a viable process chain for direct mold texturing.

Two-photon polymerization lithography (TPL) provides a suitable experimental platform to address these aspects. Based on direct laser writing and two-photon absorption, TPL enables the high-accuracy fabrication of complex three-dimensional optical micro- and nanostructures with ≈100 nm spatial resolution [7,8]. Its flexibility allows systematic variation of key geometrical parameters, making it particularly suitable for controlled parametric investigations and rapid prototyping [6].

In this work, TPL was used to study the effect of key DOE parameters, pixel pitch and phase discretization, on holographic image quality. Fabricated DOEs were first geometrically and functionally characterized to quantify the relationship between feature dimensions and image quality, thereby identifying an optimal trade-off between manufacturability and surface functionality. Subsequently, hologram robustness was evaluated by introducing controlled errors in pixel pitch and height to simulate manufacturing defects, and the results were compared with mold nanotexturing capabilities to define a geometry suitable for IM integration [4]. Overall, the study provides quantitative design guidelines for robust DOE-based anti-counterfeiting features in IM polymer components.

2. Materials and methods

2.1. DOE Design

The DOE design begins with the selection of a target image (Fig. 1a). The NBS 1952 resolution test chart was chosen due to its low sensitivity to the zero-order spot and its extended line features, which facilitate the identification of aberrations in the

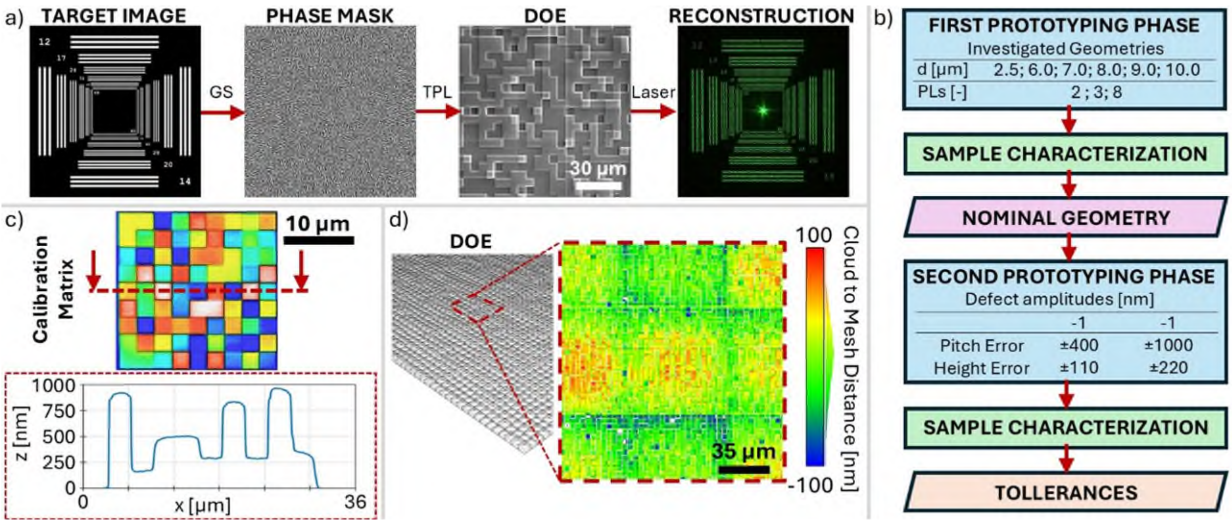

Figure 1. Surface design and validation: (a) DOE design workflow; (b) prototyping process workflow; (c) calibration matrix verification through profile analysis; d) DOE verification using point-cloud–to-mesh distance.

projected image. The target image, initially 2600 × 2600 pixels, was first resized to match the DOE footprint of 2.4 mm × 2.4 mm. A phase mask was then computed from this resized image using the Gerchberg–Saxton (GS) algorithm with 200 iterations and a 50-pixel padding to minimize edge effects. Finally, a height map was calculated by applying eq. 1 to each pixel of the phase mask:

$$h = (\Delta\phi \cdot \lambda) / (2\pi(n-1)) \quad \text{(eq.1)}$$

where $\Delta\phi$ is the phase shift assigned to the pixel, h is the corresponding pixel height, λ is the wavelength of the incident light, and n is the refractive index of the polymerized resin.

The GS algorithm with eq.1 yields continuous phase modulation from −π to +π, which was quantized into finite phase levels (*PL*s) due to the layer-by-layer TPL process. Finally, each pixel was given a nominal lateral dimension (*d*) in the X–Y plane.

2.2. TPL Process

Two-photon polymerization lithography (TPL) uses a focused laser to polymerize a photosensitive resin via two-photon absorption [8]. All DOEs were fabricated using a Photonic Professional GT system (Nanoscribe GmbH) equipped with a 63×/1.4 objective and the negative-tone photoresist IP-Dip2 (n = 1.55), on 25 × 25 × 0.7 mm fused silica substrates. A 0.6 µm base layer was added beneath each printed structure to enhance adhesion and compensate for any interface detection errors or plane tilt [7]. After printing, samples were developed in propylene glycol monomethyl ether acetate (PGMEA) for 12 min and rinsed in isopropyl alcohol (IPA) for 2 min.

All DOEs were printed using the same process parameters: laser power of 21.25 mW, beam scan speed of 20 mm/s, slice distance of 120 nm, and hatch distance of 200 nm. The process parameters used were selected to maximize printing accuracy.

2.3. Prototyping Phases

The DOE prototyping was organised in two phases (Fig.1b): (i) study of the effect of DOE geometry (*d* and *PL*) on functional performance, and (ii) study of the effect of defects on image reconstruction. In both stages, the DOEs' footprint was fixed at 2.4 mm (±50 µm), fully inscribed within the 3.5 mm laser beam.

In the first stage, 14 DOEs were fabricated with characteristic dimensions *d* ranging from 2.5 to 10 µm and phase levels of 8, 3, and 2, corresponding to minimum height steps of 120, 320, and 480 nm, respectively. Three 9x9-pixel matrices (referred to as "calibration matrices") matching each DOE geometry were printed alongside the samples to monitor TPL stability (Fig. 1c).

In the second prototyping stage, a reference DOE (*d* = 7 µm, *PL* = 3) was systematically perturbed following a full-factorial design of experiments (Fig. 1b). To simulate manufacturing defects, constant absolute deviations, evenly split between positive and negative values, were applied to 66% of randomly selected features. Specifically, height errors modified the nominal pixel heights, while pitch errors altered the widths (*d*) of randomly chosen rows and columns. The error magnitudes were based on current mold nanotexturing precision limits.

2.4. Sample Characterization

All printed surfaces (calibration matrices and DOEs) were evaluated using a confocal profilometer (Plu Neox, Sensofar; 100× objective) to quantify printing accuracy.

The calibration matrices were analyzed via a point-cloud-to-CAD comparison conducted with CloudCompare software, which mapped local deviations by comparing profilometer scans against the nominal STL geometries. To ensure measurement reliability, surface profiles were extracted at pixel centers to evaluate the pixel heights (Fig. 1c). Each of the 3 matrices printed for each geometry was geometrically characterized.

Printing accuracy of the DOEs was then assessed using the CAD comparison approach. For each DOE, two 0.5 × 0.5 mm areas relating to the start and end of the printing were scanned. From each scan, a 100 × 100 µm sub-area was extracted and compared with the nominal mesh. Results are reported as the mean and standard deviation of the distances (Fig. 1d).

The optical performance of each fabricated DOE was evaluated by analyzing its reconstructed holographic image. Each sample was mounted on an alignment system, centered in a DPSS laser beam (λ = 532 nm, power = 4.5 mW, beam diameter = 3.5 mm), and projected onto a planar screen located 3.1 m away in a light-controlled environment. Finally, the images were captured under identical exposure settings using a Raspberry Pi 5 system equipped with an HQ camera and a 16 mm lens.

The quality and sharpness of the images were evaluated using contrast (*c*) and mean squared error (MSE). Optical metrics were calculated and averaged over 3 image acquisitions per sample.

Contrast was computed for the line-pair groups (numbered 12, 17, 24, 34, 48, and 68 from the NBS calibration chart in Fig. 1a) located in the upper-right quadrant of the target image using the Michelson contrast definition:

$$c = (I_{max}-I_{min})/(I_{max}+I_{min}) \quad \text{(eq.2)}$$

where I_{max} and I_{min} are the maximum and minimum intensity values sampled along the considered line pair.

Finally, the MSE was computed via a pixel-by-pixel comparison between the reconstructed image and a reference photograph of a physical target matching the holographic image dimensions. This approach yields an MSE value independent of the acquisition system's resolution.

3. Results

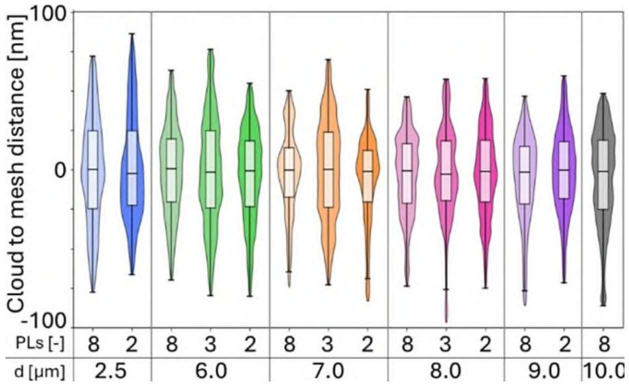

Figure 2. Calibration matrix validation through point cloud.

Comparisons between profile and point-cloud–to–mesh measurements showed no systematic trends, and differences were often within the instrument uncertainty (4–8 nm). This indicates that CAD-based comparison is a reliable method for verifying DOE dimensions. Figure 2 presents violin plots of the geometric deviation distributions measured on the calibration matrices through the CAD-comparison approach. Larger deviations are mainly associated with smaller pixel pitches, primarily due to edge effects at pixel margins, which become less significant as *d* increases. For all samples, the interquartile range lies within ±25 nm, and 95% of the data fall within ±75 nm. These deviation levels are consistent with literature values, although printing accuracy is often assessed only indirectly [6,9].

The geometric verification of the DOEs showed a mean error of approximately 0 nm across all surfaces. Standard deviation ranged from 57 nm for the DOE with *d* = 7 µm and *PL*s = 2 to 67 nm for with *d* = 2.5 µm and *PL*s = 8. No statistically significant trends were observed, and the variation in standard deviations was considered negligible. Compared with the calibration matrices, the standard deviation increases by approximately 35 nm for the DOEs. This increase is attributed to the stitching strategy of the TPL system: because DOE dimensions exceed the objective writing field, fabrication requires stitching multiple adjacent fields (Fig.1d) [8]. The resulting overlaps introduce local imperfections, while minor laser power fluctuations and uncertainties in detecting the FS–resin interface can further cause defects and misalignments between writing fields [7].

Overall, process accuracy remains stable across different geometries and over time (Fig. 2), and variations in process precision and accuracy do not significantly affect the functional performance of the individual DOEs.

The functionality of all DOE printed in the first prototyping stage was evaluated. MSE results are reported in Fig. 3a; a marked increase in MSE is observed for *d* ≥ 9 µm, due to reduced phase and image discretization and to the contraction of the high-intensity region, which increases the relative noise contribution at the center of the reconstructed image [5,6]. In contrast, MSE variations are limited for *d* = 6–8 µm, indicating more stable reconstruction quality and the growing influence of the acquisition system's background noise, which becomes comparable to the decreasing background noise in the diffraction pattern. A systematic increase in MSE is also observed with decreasing *PL* number, due to reduced diffractive efficiency [5,10]. Among the tested configurations, the 3-*PL* DOE represents a practical compromise, offering better image quality than 2 *PL*s while holding lower fabrication complexity than 8 *PL*s.

Figure 3b shows the contrast transfer functions (CTFs), obtained by plotting the contrast of line pairs in each group of the target chart versus the line-pair period of the original image. A contrast threshold of 0.3, experimentally determined as the minimum for visual distinguishability, is overlaid on the curves. In all cases, line-pair contrast decreases with increasing lines' spatial frequency. When evaluating the influence of geometric parameters, a progressive reduction in contrast is observed as *d* increases. Consistent with previous results (Fig. 3a), DOEs with a *d* ≥ 9 µm produce images with markedly inferior quality. It is also observed that DOEs with 2 *PL*s generally yield lower image sharpness than those with 8 *PL*s. However, DOEs with 3 *PL*s exhibit contrast values for line groups, up to 1.0 line pairs per 100 pixels, comparable to those obtained with 8 *PL*s. These findings indicate that a 3-level phase discretization is sufficient to preserve good image sharpness and visibility of line pairs. Nevertheless, as the phase discretization becomes coarser, noise increases in the central region of the reconstructed image and in the areas between adjacent groups (Fig. 3a).

Based on these results, DOEs with *d* = 6 and 7 µm and 3 *PL*s represent optimal compromises, with *d* = 7 µm preferred due to higher compatibility with industrial manufacturing constraints [4]. This choice is supported by the indefinable lines in the group with 1.0 line pairs per 100 pixels for *d* = 8 µm and 3 *PL*s (Fig. 3b).

The selected surface serves as a reference for the second prototyping phase (Fig. 3a). Because preliminary tests showed a complete loss of the holographic image when ±220 nm height errors affected 66% of the pixels, deviations of ±110 nm and ±220 nm were applied in equal numbers. This specific condition is denoted as '±220 nm' in Fig. 4. ANOVA of the design of experiment indicated that both defect types significantly affect *c* and MSE, while their interaction was not statistically significant. Figure 4a presents the main effects of pixel pitch and height defects on the MSE of reconstructed images. As expected, increasing deviation amplitudes reduces optical performance, with a pronounced decrease in MSE at higher defect levels, which is unacceptable due to increased noise and reduced image contrast (Fig. 4a). In particular, the hologram response strongly depends on the type of defect introduced. Height errors primarily increase background noise, mainly due to incorrect phase modulation [6,11]. While errors in the lateral dimensions induce image asymmetries, leading to the loss of visibility of one half of the line-pair groups along the image diagonal, this effect is ascribed to local changes in phase and diffraction angle [5,11].

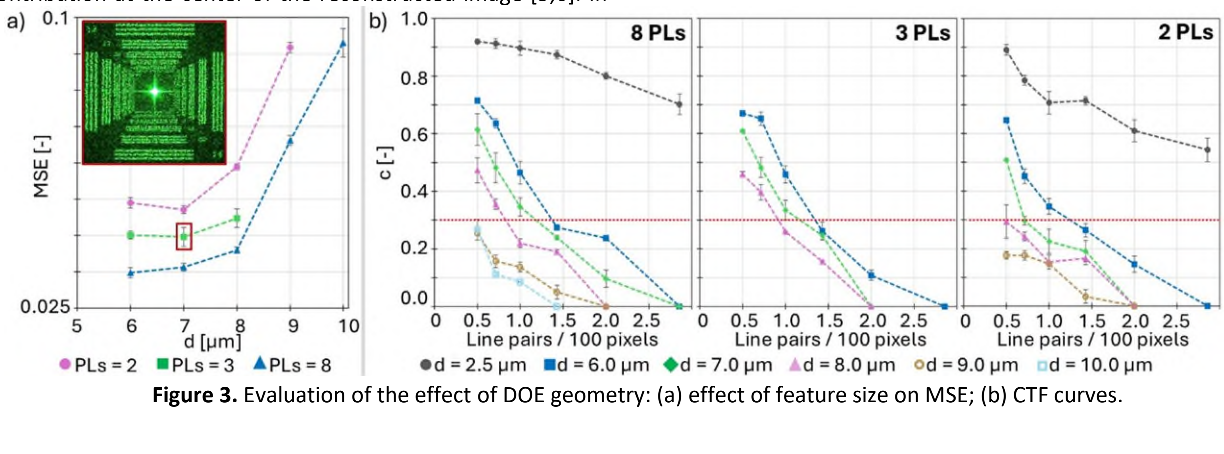

Figure 3. Evaluation of the effect of DOE geometry: (a) effect of feature size on MSE; (b) CTF curves.

Figure 4b presents the mean CTFs for reconstructed images obtained after introducing defects on the diffractive surface, with amplitude equal to the first level investigated (Fig. 1b). The maximum standard deviation for *c* in samples of the second prototyping phase is 0.04 (consistent with Fig. 3b). Notably, the addition of either pitch or height defects alone reduces the mean *c* within individual line groups but does not compromise the visibility of any group. However, the simultaneous introduction of both defect types results in a loss of visibility of the lines in the group with 1.0 line pairs per 100 pixels.

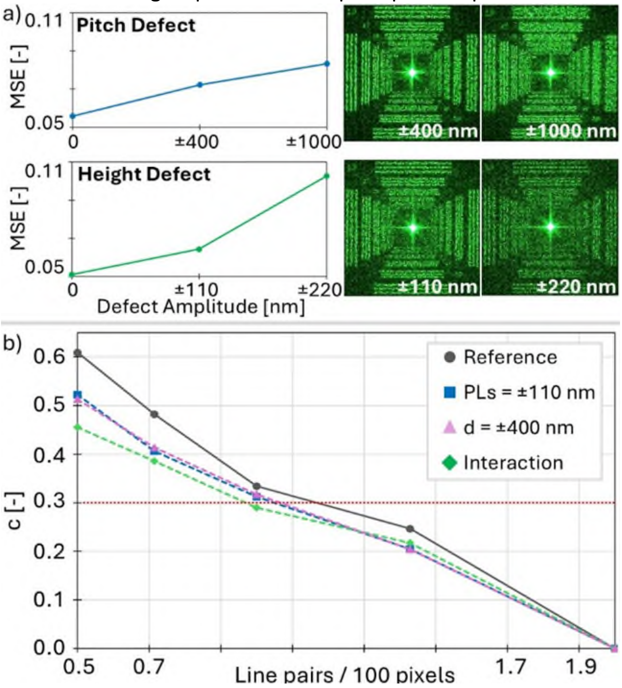

Figure 4. Effect of manufacturing defects: (a) MSE main effects plots; (b) CTF curves of DOEs with defects.

4. Discussion

From both economic and technological perspectives, laser ablation is the most viable process for producing the desired mold surface, with femtosecond (fs) laser machining providing superior control over ablation volume and improved surface quality [4,12]. Few studies have reported DOE fabrication via fs-laser processing of materials such as sapphire or quartz [9,13], typically using UV wavelengths and high numerical aperture (NA) optics to limit ablation depth and achieve tight focusing. While suitable for mold inserts, these materials are costly, and high-NA systems are not widely available industrially. More recent work on UV fs-laser ablation of conventional mold materials using low-NA optics has demonstrated ablation depths (≈320 nm) and lateral feature sizes (≈7 µm) compatible with DOE requirements, with similar spatial resolutions achieved using single-pulse fs-laser processing at longer wavelengths [12,14]. However, low-NA systems may require beam shapers to obtain square, flat-top intensity profiles.

Fs-laser ablation precision is typically ±70 nm [9,13], so the defect amplitudes considered in this study are conservative and representative of industrial conditions, including polymer shrinkage. Lateral pixel-size defect magnitudes were chosen based on the precision and accuracy of positioning systems typically employed in fs-laser platforms [9,14]. To maintain image sharpness, positioning errors should be kept within ±400 nm, requiring the laser system to be equipped with nanoscale positioning and control capabilities.

Analysis of manufacturing accuracy relative to image sharpness highlights the range of images that DOEs can effectively project and the achievable quality of holographic images. These results are particularly relevant for anti-counterfeiting, where reliable reconstruction of patterns with varying visual complexity enables encrypted security codes [2,3].

5. Conclusions

This work presents a systematic prototyping strategy to evaluate the integration of DOEs as anti-counterfeiting features in IM polymer components, considering both optical performance and manufacturing constraints. Quantitative analysis of pixel pitch and phase discretization identified an optimal trade-off between image quality and manufacturability, with DOEs featuring a 7 µm pixel pitch and 3 phase levels delivering robust holographic performance. The robustness of this configuration against realistic manufacturing defects confirms its compatibility with fs-laser mold texturing. Overall, the methodology provides practical design guidelines bridging optical design and industrial fabrication. Future work will investigate surface roughness and polymer shrinkage–induced refractive index variations to further refine DOE integration.

References

[1] Sorgato, M., Baruffa, G., Oubellaouch, K., Zaniboni, G., & Lucchetta, G. (2025). A novel method for high-volume manufacturing of self-protective plastic surfaces to ensure durable anti-counterfeiting functionality. *CIRP Annals*, **74**, 783-787.

[2] Ruffato, G., Rossi, R., Massari, M., Mafakheri, E., Capaldo, P., & Romanato, F. (2017). Design, fabrication and characterization of computer generated holograms for anti-counterfeiting applications using OAM beams as light decoders. *Scientific reports*, **7**(1), 18011.

[3] Mohammad, N., Meem, M., Wan, X., & Menon, R. (2017). Full-color, large area, transmissive holograms enabled by multi-level diffractive optics. *Scientific reports*, **7**(1), 5789.

[4] Masato, D., Piccolo, L., Lucchetta, G., & Sorgato, M. (2022). Texturing technologies for plastics injection molding: a review. *Micromachines*, **13**(8), 1211.

[5] Taghizadeh, M. R., Blair, P., Layet, B., Barton, I. M., Waddie, A. J., & Ross, N. (1997). Design and fabrication of diffractive optical elements. *Microelectronic Engineering*, **34**(3-4), 219-242.

[6] Wang, H., Liu, Y., Ruan, Q., Liu, H., Ng, R. J., Tan, Y. S., ... & Yang, J. K. (2019). Off-Axis holography with uniform illumination via 3D printed diffractive optical elements. *Advanced Optical Materials*, **7**(12), 1900068.

[7] Wang, H., Wang, H., Zhang, W., & Yang, J. K. (2020). Toward near-perfect diffractive optical elements via nanoscale 3D printing. *ACS nano*, **14**(8), 10452-10461.

[8] Wang, H., Zhang, W., Ladika, D., Yu, H., Gailevičius, D., Wang, H., ... & Yang, J. K. (2023). Two-photon polymerization lithography for optics and photonics: fundamentals, materials, technologies, and applications. *Advanced Functional Materials*, **33**(39), 2214211.

[9] Li, Q. K., Chen, Q. D., Niu, L. G., Yu, Y. H., Wang, L., Sun, Y. L., & Sun, H. B. (2016). Sapphire-based Dammann gratings for UV beam splitting. *IEEE Photonics Journal*, **8**(6), 1-8.

[10] Pavelyev, V., Osipov, V., Kachalov, D., & Chichkov, B. (2013). Diffractive optical elements with radial four-level microrelief fabricated by two-photon polymerization. *Optics Communications*, **286**, 368-371.

[11] Roeder, M., Schilling, P., Hera, D., Guenther, T., & Zimmermann, A. (2018). Influences on the fabrication of diffractive optical elements by injection compression molding. *Journal of Manufacturing and Materials Processing*, **2**(1), 5.

[12] Genieys, T., Sentis, M., & Utéza, O. (2020). Measurement of ultrashort laser ablation of four metals (Al, Cu, Ni, W) in the single-pulse regime. *Advanced Optical Technologies*, **9**(3), 131-143.

[13] Stonyte, D., Jukna, V., Lukosiunas, I., Zakarauskas, P., Huang, H. H., Katkus, T., ... & Paipulas, D. (2024). Four-level diffractive photon sieves by deep-UV femtosecond laser ablation. *Optics Express*, **32**(24), 43102-43117.

[14] Buchner, B., Mittelmann, S., von Toussaint, U., & Neu, R. (2025). Investigation of UV-Femtosecond laser ablation on metallic substrates. *Applied Physics A*, **131**(9), 693.